EUROPEAN ORGANIZATION FOR NUCLEAR RESEARCH

CERN–PPE/93–209
1 November 1993

FAST RICH DETECTOR WITH A CAESIUM IODIDE PHOTOCATHODE AT ATMOSPHERIC PRESSURE

A. Braem[b)], A. DiMauro[a)], E. Nappi[a)], A. Ljubicic Jr.[c,*)], G. Paic[b,c,*)], F. Piuz[b)], F. Posa[a)], R.S. Ribeiro[b)], T. Scognetti[a)] and T.D. Williams[b)]

Abstract

CsI photocathodes of 30 × 30 cm^2 size have been operated in a fast RICH detector composed of a NaF radiator and a multiwire proportional chamber with a cathode-pad readout. Results are presented from tests with a 3 GeV/c proton beam. A Cherenkov angular resolution of 8 mrad is obtained by detecting a mean of 8 photoelectrons per ring. Methods are described for counting the Cherenkov photons and evaluating the differential quantum efficiency of the CsI photocathode. The results obtained with photons impinging at a large angle on the CsI layer are presented and discussed in comparison with higher quantum efficiencies observed under different experimental conditions.

Presented at the First Workshop on RICH Detectors,
2–5 June 1993, Bari, Italy
Proceedings to be published in Nuclear Instruments and Methods A

a) INFN and Politecnico, Bari, Italy.
b) CERN, Geneva, Switzerland.
c) R. Boskovic Institute, Zagreb, Croatia.
*) Supported in part by a grant from 'Open Society'.

1 INTRODUCTION

Since the publication of Seguinot et al. [1] reporting evidence for a significant quantum efficiency (QE) of thin layers of CsI operating in gas counters, a great deal of activity has been carried out to understand the full potential of such photocathodes (PCs) for UV light detection primarily for Ring-Imaging Cherenkov (RICH) counter applications. Although the QE reported in Ref. [1] is somewhat lower than the values for tetrakis(dimethylamine)ethylene (TMAE), such PCs would considerably ease the use of RICH detectors. We enumerate the simplifications we believe are of importance:

- the possibility of using very thin sensitive gaps dominated by the gain and stability requirements of the detector rather than by the mean free path of the UV photons in the gas, as is the case when using photosensitive vapours,
- elimination of the need for a window in front of the UV detector in the case of proximity-focusing devices (solid or liquid radiator),
- photoconversion in a single plane without parallax,
- no hazards linked to heating and condensation of TMAE,
- increased transparency in the detector entrance electrode, due to the fact that the requirements for the uniformity of the electrical field may be relaxed since the photoelectrons are created only in one plane at the PC.

In the past few years, many groups have studied the QE of CsI [2]. Although very important, these studies have, by nature, different experimental conditions from their final use in RICH counters. The differences are manifold: the polarization of the Cherenkov light, the angle of incidence, the single-electron detection mode [multiwire proportional chamber (MWPC)], the area of the PC, the latitude in the choice of a substrate. Several experiments proposed by the heavy-ion community [3] envisage systems of very large area for particle identification in a low-momentum range (0.8 to 3 GeV/c) and with very high multiplicity (40–60 tracks/m^2). Such requirements impose a specific fast RICH layout where a CsI PC is mandatory. Therefore, we have decided to test the behaviour of CsI PCs under RICH operating conditions, aimed at satisfying the previous criteria in terms of particle separation capability [4] and of technical feasibility as well as contributing to intrinsic studies of the CsI PC properties.

Recently, we have reported [5] on the test of a 10 × 10 cm^2 RICH operating with CsI PCs on a pad readout plane of a MWPC at atmospheric pressure. Other studies on CsI/RICH operation are described in Ref. [6]. In the present paper, we summarize the results obtained with 30 × 30 cm^2 CsI PCs using the same technique. We shall report on the construction of the detector as well as on the results obtained with a NaF radiator, which allows an appraisal of the differential QE for the CsI as measured in a real detector.

2 DESCRIPTION OF THE EXPERIMENT

Our apparatus and associated electronics were already described in Refs. [5] and [7], where CsI photocathodes and gaseous photoconverters [TMAE or triethylamine (TEA)] were used respectively. We briefly review the main features:

i) *The RICH detector*

A proximity-focusing geometry is used as sketched in Fig. 1. It consists of:

- The radiator array, a NaF plate, 10 mm thick and 50 mm in diameter, whose distance to the pad plane can be varied *in situ*. A wire electrode of 4 mm pitch is fixed close to the plate and polarized so as to collect the primary ionization deposited by the charged particles in the proximity gap,

- The photon detector made of a MWPC whose geometry is described in Fig. 1. The full size of the detector is 50×50 cm^2 but the pad cathode on which the CsI evaporation was performed has a sensitive area of 40×36 pads of 8×8 mm^2 size. The detector was flushed either with pure methane or with a mixture of methane/isobutane, 95/5 in volume. The gas was circulated at 20 l/h, passing through Oxysorb and Hydrosorb cells with oxygen trace monitoring. The system was submitted to the variable temperature/pressure conditions of the experimental hall.

ii) *The electronics and data acquisition*

An analog multiplexed system is used, composed of the VLSI-Cmos AMPLEX [8] as the front-end chip and the DRAMS card [9] performing the readout at a multiplexing rate of 500 kHz on an 8 bit FADC. Data were taken in a way that all pads were read out at every event. A pedestal run allows to define and vary off-line the threshold value to be applied at every pad. These values are defined according to the relation thr(i) = pd(i) + N* sig(i), where pd(i) and sig(i) are respectively the mean and the r.m.s. values of the i-th pedestal distribution and N, a variable number. The equivalent charge noise is 1800 $\pm$ 300 electrons.

iii) *The CsI photocathode*

The CsI layers are evaporated onto the pad cathode made of a standard printed board etched on a G10 substrate and protected with gold deposited chemically on copper. Owing to the respective electrode and vacuum vessel sizes, the evaporation was performed from four boats located below the four electrode corners, at 40 cm distance. The boats were loaded with the amount of CsI necessary to achieve a 0.5 μm thickness after evaporation. The four boats were operated together and the deposition rate was controlled with two quartz balances. A variation in thickness of about 10% is expected from such a procedure. The evaporation is started with the boats covered by shutters and is carried on at a pressure of $2 \times 10^{-6}/7 \times 10^{-7}$ Torr. No heating procedure was performed under vacuum. The transfer of the PC from the vacuum vessel to the detector implies an exposure to air of about 10 minutes plus the time needed to flush air out of the detector. The evaporated CsI material was either powder or crystal.

iv) *Beam and control*

The data were taken at the CERN/PS/T11 extracted beam, composed of pions/protons at 3 GeV/c momentum. A time-of-flight system allows for on- and off-line particle identification. The event trigger selection is provided by the fourfold time coincidence of scintillators defining an acceptance of 10×10 mm^2 for particles normal to the pad plane. A deuterium lamp illuminates a pad through a quartz window, allowing the study of single electrons emitted at a known location, using the sense wire as a trigger.

3 METHOD FOR THE EVALUATION OF THE CsI DIFFERENTIAL QUANTUM EFFICIENCY

The size of our present CsI PC is suitable for the generation of Cherenkov rings of up to 150 mm radius. As seen in Fig. 2, the photoelectrons are well separated and can easily be identified according to a procedure described later on. Using the NaF refractive-index dependence on photon energy [10], the distances between the impact points of the particle (ring centre) and of a photon of energy E are calculated as a function of E, for protons of 3 GeV/c and for the distances radiator-to-pad plane in use during the tests. The result, shown in Fig. 3, indicates that, owing to the high chromaticity of the NaF radiator, the photon energy can be evaluated with a resolution increasing with the photon energy. With particles of $\beta = 0.9544$ (3 GeV/c proton), the maximum energy of photons emitted

from the NaF radiator before total reflection occurs is 8.2 eV. Of course, approaching this energy, an increasing fraction R of photons is reflected at the NaF/gas interface according to:

$$R = [tg(\theta_c - \theta_e)/tg(\theta_c + \theta_e)]^2 \quad \text{where} \quad \cos\theta_c = 1/n\ \beta \quad \text{and} \quad \sin\theta_e = n\ \sin\theta_c\ . \qquad (1)$$

θ_c is the Cherenkov angle, this radiation being taken as p-polarized.

These remarks define our procedure for QE evaluation as follows:

- Given a particle velocity, a distance pad/radiator, and a radiator thickness, two concentric rings are defined in the pad plane, whose radii correspond to some minimum and maximum photon energies according to the NaF chromaticity curve. The location of the Cherenkov photon emission is taken at the middle of the radiator plate. These circles define a fiducial zone for photon counting corresponding to a total photon energy range, ΔE.
- The total range of the fiducial zone is subdivided, according to Fig. 3, into concentric zones of 0.25 eV width, the photoelectrons being counted in the ring area between the corresponding circles. We assume that the different quantities, dependent on the photon energy such as photon-loss coefficients $\Pi[\varepsilon_{loss}(E_n)]$ and QE, are about constant within this small energy range. For a value E_n, centred in the energy bin n, we can write the approximate relation:

$$QE(E_n) = N_{phel}(E_n)/\{370\ \sin^2\theta_c(E_n)\ \Pi[\varepsilon_{loss}(E_n)]\ \varepsilon_{det}\ \Delta E\}\ , \qquad (2)$$

  where $N_{phel}(E_n)$ is the number of photoelectrons counted in the zone E_n, ε_{det} the single electron detection efficiency, and $\Delta E = 0.25$ eV.

The spread of the photon emission along the particle path in the radiator makes this method approximate unless very thin radiators are used. The influence of the proximity-focusing error in the 10 mm radiator thickness is illustrated in Fig. 4, where the distributions of the photon impact points are plotted for photons generated across the radiator, at energies drawn within consecutive bins of 0.25 eV width. This plot indicates that the geometrical error can be translated into a spread of the energy associated with every bin; the higher the energy, the smaller the spread. Our detector response simulation programme (see Section 7) has been used to evaluate this spread. Photons are generated in the radiator within 0.25 eV energy bins and propagated through the real detector (all losses, QE, signal generation, etc., taken into account). At every photon impact at the pad plane, the corresponding energy is recalculated, providing a new energy distribution whose r.m.s. value is taken as the energy spread.

4 PHOTON COUNTING

It is expected that a certain fraction of the clusters of pads originates from more than a single electron, i.e. the resulting pad pulse height (PH) pattern is the convolution of two or more single-electron PH patterns. Their origins could be either close Cherenkov photons, or close photon feedback associated with a Cherenkov photon avalanche or noise. In order to achieve the deconvolution of such PH patterns and resolve them, the spread of the charge induced at the pad electrode has been measured in the present chamber configuration [7], [11].

We describe the ring event analysis procedure, illustrated by experimental results of a particular run (run 50, threshold at N = 3.5, see Section 5.2):

i) All electronic thresholds are calculated from the pedestal distributions by fixing the value of $N > 3$ (Section 2). A few noisy channels are suppressed ($< 0.5\%$).

ii) The total number of pads hit per event is counted in the total fiducial zone, providing a distribution as shown in Fig. 5a.

iii) A search is made to find raw clusters of pads, defined as having only adjacent edges. Configurations with common corners are forbidden by our pad/wire configuration and the spread of the induction. The distributions of the size of the raw clusters and the number of raw clusters per event are shown in Figs. 5b and c.

iv) At present, the raw clusters are classified and attributed a number of electrons in the following way:
   - class 1 = one electron: cluster size of 1, 2 and 3 pads when the pad having the maximum PH is not at an end of the PH pattern,
   - class 2 = two electrons: cluster size of 3 pads when the pad having the maximum PH is at the end of the PH pattern,
   - class 3 = two electrons: cluster size of ≥ 4 pads.

The location of the electron is taken at the middle of the pad having the maximum PH. The distributions of number of resolved clusters per event and size of resolved clusters are shown in Figs. 5b and c.

The method just described results in PH distributions for these three classes as expected:

i) The total pad PH/cluster of class 1 gives an exponential Fury distribution as expected from single electrons (Fig. 6a), which would not be the case if class 2 and class 3 were mixed. Since these distributions are obtained using an external trigger (scintillators), the threshold cut, A_{th}, is found to be very sharp (one bin) (Fig. 6b) Since no Polya behaviour has been observed at our operating voltages, we therefore use as the single-electron detection efficiency the relation $\varepsilon_{det} = \exp(-A_{th}/A_0)$. A_0 is obtained from an exponential fit to the PH/class 1 distribution, started at A_{th}.
   On the contrary, the total pad PH/cluster of class 2 or 3 shows the statistical behaviour expected from events composed of more than one initial electron since the distribution is now peaked and not any more exponentially shaped (Figs. 6c and d).

ii) From this discussion, some conclusions can be drawn about the presence of photon feedback. A simple simulation allows the prediction of the probability of having class 2 and class 3 clusters. An expected number of photoelectron impact points is generated in the fiducial zone, with a cluster size of the class 1 distribution. The fraction of clusters having overlapping and adjacent PH patterns is extracted. Depending on the high voltage (cluster size), this fraction is found to amount to 5–6%. Since the measured fraction of clusters of size > 3 in classes 2 and 3 is found to be 7–9%, we estimate that a photon feedback contribution is present in about 2–4% of the total number of clusters. This observation is supported by measurements made with single electrons locally generated by a UV source. Applying the same cluster classification, we observed that, at a given voltage:
   - The same slope A_0 is obtained as for the Cherenkov photoelectrons.
   - A 1–2% fraction of correlated, separated clusters (no adjacent edge, but corners allowed) is found, having an exponentially shaped PH distribution. It is then assumed that these clusters originate from photon feedback.

Since the aim of this analysis is to evaluate the number of photons for QE evaluation purposes, the present uncertainty on their localization is of minor importance. For

example, some unknown fraction of class 1 clusters (< 5%) may consist of two-photon events as well, without affecting the QE evaluation.

In a further analysis, we shall be able to resolve all clusters of size ≥ 2 with more accurate localization by applying the PH pattern deconvolution technique [11]. An evaluation of the systematic error made on the Cherenkov ring angle determination will then be possible since some of the photon feedback candidates will be recognized.

5 RESULTS

5.1 Operation of the detector

Three large PCs were evaporated. The same pad substrate was used after removal of the previous deposit by cleaning with water and dry alcohol. Mounted on the detector, the PCs were in operation for several months, exposed to a particle rate of about 0.5–1 kHz/cm^2 in a central zone of about 100 cm^2. No 'HV conditioning' period was necessary at their first operation; neither stray currents nor sparks were observed during the whole of the operation with or without isobutane admixture.

The mean number of pads hit by charged particle is 4.2 at the maximum operating voltage (2.10 kV).

By superimposing about 2000 rings in two-dimensional plots, we have observed inhomogeneities in the local density of Cherenkov hits showing reproducible patterns for different PCs. It has been proved that this effect was not due to the PC performance as initially supposed. By moving the detector in the beam or rotating the radiator, these patterns were found to be correlated with the NaF radiator transmission. A polishing of the NaF plate was not sufficient to remove these features. The UV transmission of the plate was measured with a monochromatic UV source without reproducing the Cherenkov test features. Let us note that in one case single photons are to be transmitted, whilst in the other case an intense and wide UV beam is used. This point will be discussed further in Section 7.

5.2 Detector performance

From a large series of measurements, we now present the detailed results of three runs whose experimental conditions are summarized in Table 1.

The single electron efficiencies, the pad cluster size, the mean numbers of photoelectrons/ring, the mean number of pads hit per ring are shown in Fig. 7 as a function of the pad electronic threshold. These numbers were found to be reproducible within 5% over about 50 runs taken in a period of 5 months with three different PCs.

The centre of the rings being taken in the analysis at a fixed point in the detector, the size of the triggering scintillators introduces a ± 4 mm localization error of this point. Figure 8 shows the distributions of the Cherenkov angle and the distance to the ring centre of single Cherenkov clusters.

The ring radius is calculated in two ways: i) by taking the photoelectron localizations from the cluster resolution procedure (Section 4), ii) by averaging the distances of the centre of the ring to the centres of all pads hit in the fiducial zone. In Fig. 9, the distributions of ring radii and the associated Cherenkov angle are represented, resulting in a $d\beta/\beta$ of 0.7%. Identical results are obtained with both methods of calculating the radii.

The large spread observed on the distances was, as noted before, chosen on purpose because of the NaF chromaticity at the expense of the Cherenkov resolution performance. Keeping the present CsI QE performance, these results can easily be improved by replacing

the MWPC cathode mesh by a more transparent grid (transmission = 0.8 instead of 0.6), by gaining on the detector efficiency, and by using a liquid freon (C_6F_{14}) radiator of reduced chromaticity [12].

5.3 Evaluation of the CsI differential QE

The variations of the photon loss coefficients and their convolutions are plotted as a function of photon energy in Fig. 10 for operation with methane and methane/isobutane. We have considered: the NaF transmission (measured), the gas mixture transmission (calculated), the reflection at the NaF interface, and the mesh transparency calculated as a function of the angle of incidence.

Following the method of Section 3, the frequency distribution of the distances of the ring centre to Cherenkov clusters shown in Fig. 8 is now plotted as a function of the photon energy with a binning of 0.25 eV. Figure 11 shows the results obtained in the case of methane and methane/isobutane. The superior UV transmission of the pure methane is apparent in the frequencies of the last bins of these plots, extending up to 7.825 eV in the case of methane. To calculate the $QE(E_n)$ values, the single-electron detection efficiencies used are those quoted in Fig. 7.

The lower part of Fig. 12 shows the results obtained from the three runs of Table 1 (PC 30×30 cm^2), applying the relation (2). In our previous measurements, obtained with smaller PCs (10×10 cm^2) [5], only integrated QE values were calculated at that time. These measurements have been re-evaluated with the present analysis and the upper part of Fig. 12 shows the differential QE variation. The integrated values are found to be about 20% lower than the ones quoted in Ref. [5], one reason being that the single-electron PH spectra are now directly obtained from the Cherenkov photoelectrons and not from a UV light calibration as described in Ref. [5].

6 COMPARISON WITH A SIMULATION PROGRAMME

The detector response can be fully simulated with a programme organized as follows [12]:

i) The detector geometry and particle species are chosen according to an experimental run.

ii) Photons are generated in a given energy range ΔE along the radiator thickness L. Their number/event is drawn in a Poisson distribution of mean ($370\ \sin^2\theta_c\ \Delta E\ L$). Their location is taken as a flat distribution of width L.

iii) All photons are propagated through the detector, submitted to the losses described in Fig. 10.

iv) A number of photons are converted at their impact points on the pad/wire array, according to a QE curve,

v) PH pad patterns are generated for every photoelectron according to a single-electron PH spectrum of mean A_0 and the shape of the spread of the induced charge. All PH patterns are superimposed per ring event and every pad PH value compared with a threshold value, A_{th},

vi) The generated events are passed through the experimental analysis programme with a convenient definition of the fiducial zones.

Choosing the measured CsI QE (Fig. 12) and single-electron PH spectrum, the simulation reproduces well the mean and r.m.s. values of the current experimental distributions, such as number of pads hit/event, of cluster/event and photoelectrons/event. In addition, the frequency distribution of the distances ring centre – Cherenkov cluster

is correctly reproduced when plotted against both distance and photon energy. Using, in the simulation, different gas transparency curves shows the sensitivity to this parameter (Fig. 13).

As stated in Section 3, this programme was used to calculate the error made on the photon energy when evaluating the differential QE in narrow energy bins.

7 DISCUSSION

As quoted in the Introduction, a large number of QE measurements [2] have recently been performed with monochromatic UV beams, about normal to the CsI sample, measuring either direct photocurrent or using ionizing chamber techniques. It is difficult to characterize the polarization of such UV beams, since it depends on specific details of the layout. At the moment, the results exhibit a large spread, of a factor of 2 to 3, mainly in the low photon energy range. At the present state of analysis, our last measurements are close to the lowest QE values found in these studies.

As described in Section 5, the most important experimental uncertainty of the present QE evaluation comes from the radiator transmission. Even by moving the NaF crystal, we could not get rid of an asymmetry in photoelectron density between the left and right halves of the ring. It has been checked that the single-electron PH spectra are identical on both halves. This asymmetry could contribute to a 15–20% increase of the QE if the highest density were uniform. In addition, it might well be possible that the same problem is present in the high density half. One should also consider that probable inhomogeneities of the polarizing properties of the radiator, induced for example during the crystal growth or by mechanical strains, may adversely affect the transmission of the originally polarized light.

Some other smaller error sources can be found in the evaluations of the mesh transparency (overlap of crossed wires not taken into account) and of the gas transmission. These corrections could result in an increase of about 25% of the quoted QE values.

There are other differences between the Cherenkov and UV beam QE evaluations:

i) The electrical field strength at the CsI/gas interface is in our case about 2.8 kV/cm, i.e. E/p = 0.36 V mm^{-1} Torr^{-1}. This is a low value compared with the ones used in the UV beam QE evaluations [2] but certainly cannot explain the difference between the result of Anderson et al. [2] and the present results obtained at 740 Torr.

ii) We report an observation that we believe is of interest, although it was observed only once with such an amplitude. A pad, covered with CsI, was irradiated with UV light (deuterium lamp and quartz fibre) through a slit of variable width. The rate of the single electrons was counted at an anode wire, monitoring the signal PH. In Fig. 14, we show the behaviour in time for three different slits, changed by steps (open or closed). For a given slit width, we observe that a plateau is gradually reached, either by an increase in the rate for low illumination levels or by a decrease for high illumination levels. Over a period of two hours, a plateau level was found to be about constant at a given illumination. Neither microdischarges nor sparks were observed and the mean PH, measured every two minutes, was found to be constant during this time period. It is therefore possible to correlate such a rate effect with a variation of the emissive yield of the surface. Such an effect could originate from local accumulation of positive charges at the CsI surface. Considering a gas gain of 7×10^4 and a local rate of 10 kHz, very large electrical fields (about 1×10^7 V/cm) could be achieved through a perfect insulating layer, assuming no charge leakage. This is not the case since sparks are never observed. The surface resistance and the structure

of the layer play an obvious role in the building-up of such a field, even of reduced strength, which might be of comparable influence to any 'E/p effect'.

iii) The incident angle of the p-polarized Cherenkov photons at the CsI surface ranges from 60° to 80° in the present measurements. The reflection loss factor, R, is calculated according to the relation quoted in Section 3, having extrapolated the CsI refractive index data of the Harshaw catalogue [13] and used the following polynomial fit: $n = 0.8105 + 0.32836\ E - 0.011726\ E^2$.

In the case of p-polarization, the incident angle values precisely are close to the Brewster angle where the loss is minimum. The variation of R is plotted in Fig. 15 as a function of the incident angle for p- and s-polarizations. A sharp rise is seen when the incident angle is larger than 75°, corresponding to a photon energy of 7.5 eV in the present set-up. However, it is known that the present CsI surface is far from being specular, owing to a poor substrate quality. Consequently, at any impact location, the incident angle can be altered by some angle α, making the real incidence such that the photon is reflected. The contribution of a random variation of α by $\pm 10°$ is also shown in Fig. 15. This contribution can also be oriented in such a direction that the light has an s-component in the incidence plane, submitted to a much higher loss.

Siegmund et al. have reported [14] the variation of the QE of CsI deposited on microchannel plates as a function of the incident angle and the photon energy. The maximum QE is found at angles varying between 70° and 80°, the larger angle corresponding to the higher photon energy. Although the polarization of the light used in this experiment is unknown to us, such values correspond to the Brewster angle where the reflection loss is at a minimum.

Other measurements [15], performed on CsI covered plates and using a UV beam at an incidence up to 45°, have not shown significant differences. They should be confirmed since a 20% effect is expected between 0° and 50°.

These speculations will be checked in the present set-up, generating Cherenkov photons at close to normal incidence by inclined tracks or by using gaseous radiators. The point has to be clarified soon, since it represents the main difference between the Cherenkov and UV beam QE evaluations.

8 CONCLUSION

Although, further clarifications and improvements are still required, we believe that these results allow us to draw the following preliminary conclusions:

i) Large areas (m^2) of CsI photocathode can be produced by a conventional evaporating technique on standard printed board substrates at a moderate cost.

ii) Such a PC, associated with a MWPC operated at atmospheric pressure and ambient temperature, allows the detection of single electrons with up to 90% efficiency and a two-dimensional localization in a reliable and stable operating mode. Sizes up to 50×50 cm^2 have been successfully tested in a particle beam environment.

iii) Such a PC was tested in a fast RICH configuration using a NaF radiator, 10 mm thick, which implies the detection of p-polarized photons at 70–80° incident angle. QE values of 0.10 and 0.12 are found at 7.1 eV (175 nm) and integrated over the range 5.6–7.6 eV respectively. The photon feedback contribution is found to be at the few per cent level.

iv) This QE value allows the detection of eight photoelectrons per Cherenkov ring at $\beta = 0.9455$ with a $d\beta/\beta$ of 0.7%. This result is already relevant for particle identification with a large system in future heavy-ion collision experiments.

v) This QE value matches the result given by CsI PC manufacturers [16]. It is however smaller by a factor of 2 than recent measurements performed with UV beam irradiation on small samples [2]. At the present time, these large QE variations can be correlated only with a few parameters without enough quantitative physical support. Other basic characterizations of the CsI/gas interface should be carried out, but evidently this appears to be a cumbersome task, since such a system is far from being an 'ideal' surface state. We intend to investigate the stechiometry of the surface using the ESCA technique which also allows the search for surface contaminants and the evaluation of the work functions [17]. The study of the surface resistance under UV irradiation will also provide useful information about the field at the surface.

Acknowledgements

The authors are participants in the CERN Detector Research & Development Project RD26 on 'Fast RICH and CsI Photocathodes'. It is composed of institutes from Bari, CERN, Coimbra, Giessen, Munich, Padova, Rehovot, Zagreb. They warmly thank their colleagues for many fruitful discussions and experimental participation or support: Prof. A. Policarpo from Coimbra, Drs. J. Friese and K. Zeitelhack from Munich, Prof. W. Kuehn from Giessen, Dr. P. Sartori from Padova, Drs. A. Breskin and R. Chechik from the Weizmann Institute. The financial support received from these institutes is acknowledged.

We also thank Drs. G. Malamud and Ph. Mine from the Ecole Polytechnique, Palaiseau, and Dr. P. Besson from DPIA/Saclay for having discussed and compared their own work during the course of these studies. We are grateful to Drs. D. Anderson and S. Kwan for their advice on the CsI layer processing technique and for providing us with CsI crystals.

References

[1] J. Seguinot et al., Nucl. Instrum. Methods **A297** (1990) 133.

[2] B. Hoeneisen et al., Nucl. Instrum. Methods **A302** (1991) 447;
D. Anderson et al., Nucl. Instrum. Methods **A323** (1992) 626 and **A326** (1993) 611;
H. Braüning et al., Nucl. Instrum. Methods **A327** (1993) 369;
G. Malamud et al., X-LPNHE/93-10, Ecole Polytechnique, Palaiseau.
See also, in the section 'Photosensitive materials' of these proceedings, the contributions of Drs. P. Besson, R. Enomoto, S. Kwan, C. Lu, G. Malamud, Ph. Mine.

[3] Letter of Intent for A Large Ion Collider (ALICE), CERN/LHCC/93-16.
Letter of Intent in preparation for the HADES experiment at GSI/Darmstadt.

[4] A. Ljubicic Jr. et al., these proceedings.

[5] F. Piuz et al., Nucl. Instrum. Methods **A333** (1993) 404.

[6] R. Arnold et al., Strasbourg/CRN/HE 91-06, 1991;
M. Staric et al., Nucl. Instrum. Methods **A307** (1991) 145.
V. Cindro et al., Proc. 3rd Int. Conf. on Advanced Technology and Particle Physics, Como, June 1992, in Nuclear Physics B (Proc. Suppl.) **32** (1993) 230.
See also, in these proceedings, the contributions of Drs. P. Besson, N. Lockyer M. Staric.

[7] E. Chesi et al., Nucl. Instrum. Methods **A283** (1989) 602.
F. Piuz et al., 4th San Miniato Topical Seminar, Experimental Apparatus for High Energy Physics and Astronomy, eds. P. Giusti et al. (World Scientific, Singapore, 1990), p. 121.

[8] E. de Beuville et al., Nucl. Instrum. Methods **A288** (1990) 157.

[9] E. Chesi et al., CERN/JETSET Internal note (1991).

[10] M. Hempstead et al., Nucl. Instrum. Methods **A306** (1991) 207.

[11] T. Scognetti, thesis in preparation, INFN Bari.

[12] R.S. Ribeiro, thesis in preparation, Coimbra, presented at the 3th Int. Conf. on Advanced Techniques and Particle Physics, Villa Olmo, Como, June 1992.

[13] Harshaw Chemical Co., Crystal Optics (1982).

[14] O.H.W. Siegmund et al., SPIE Vol. 687, Ultraviolet Technology (1986) 117.

[15] J. Friese RD26/T.U. Munich, private communication.

[16] Hamamatsu Corp. Photomultipliers, catalogue.

[17] C. Coluzza et al., these proceedings.

Table 1

	Run 50	Run 52	Run 18
Gas mixture	methane/isobutane	methane/isobutane	methane
Distance radiator/pad [mm]	43	43	23
Total fiducial zone [mm]	65/140	65/140	30/140
HV [kV]	2.05	2.10	2.05
Electronic gain	g	g	g/2

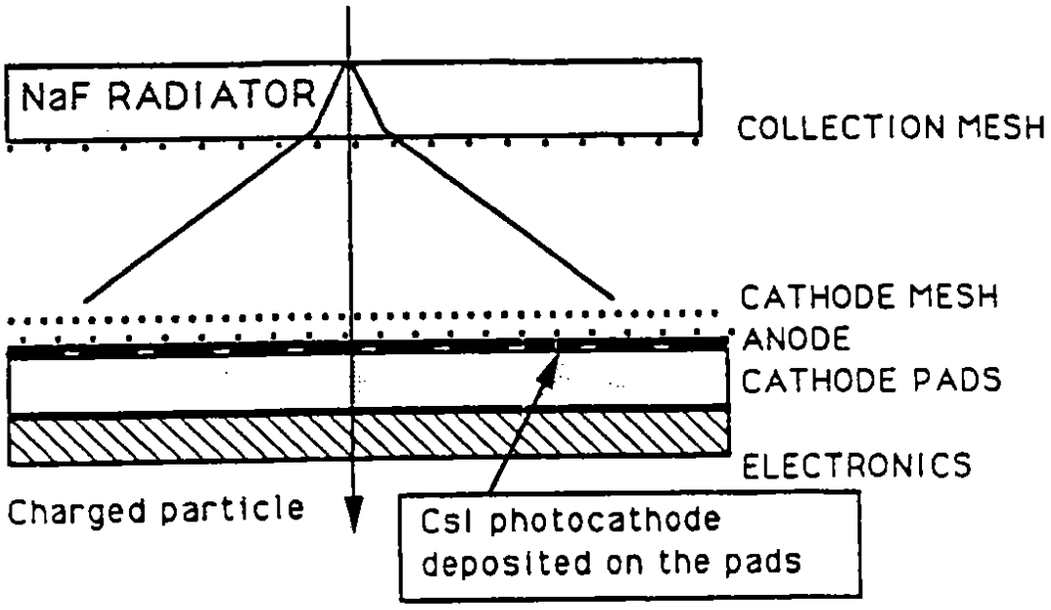

Figure 1: Sketch of the fast RICH. The MWPC is composed of i) a cathode mesh of 500 μm pitch, 50 μm wire diameter, ii) an anode plane made of 20 μm diameter wires spaced 4 mm apart, iii) a pad cathode plane. The distance cathode to anode is 2 mm. Pads, of 8×8 mm^2 size, are traversed by two anode wires located, in projection, at 2 mm from parallel edges. The distance radiator-to-pad plane is varied between 20 mm and 50 mm.

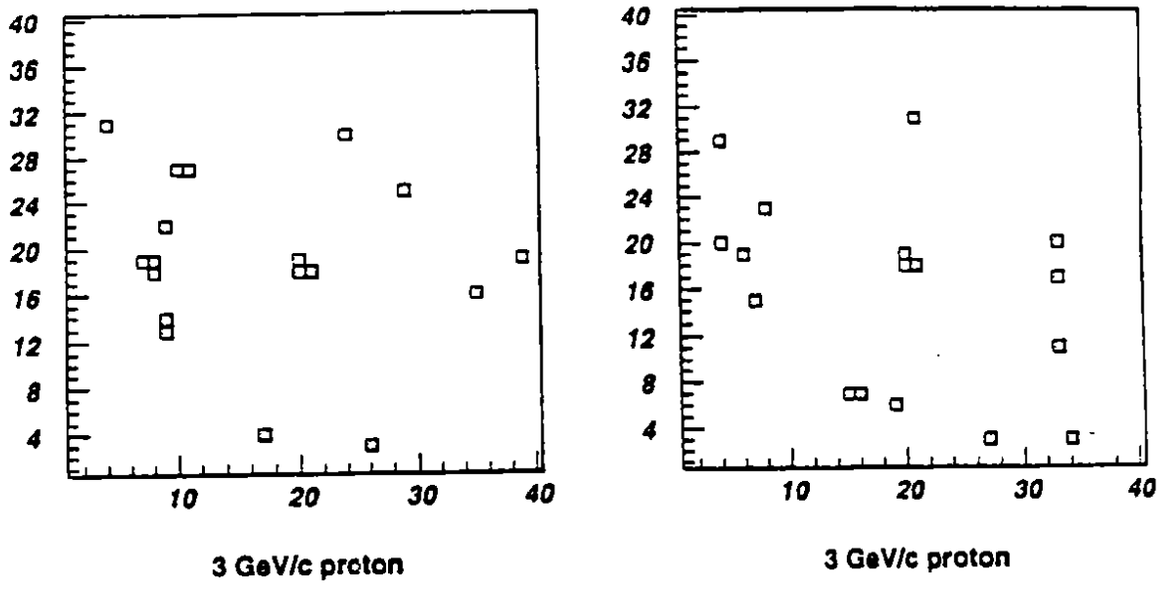

Figure 2: A single Cherenkov event: the pad cluster induced by the passage of the particle is seen at the centre, surrounded by the Cherenkov photoelectron clusters. Coordinates are in pad units (8 mm).

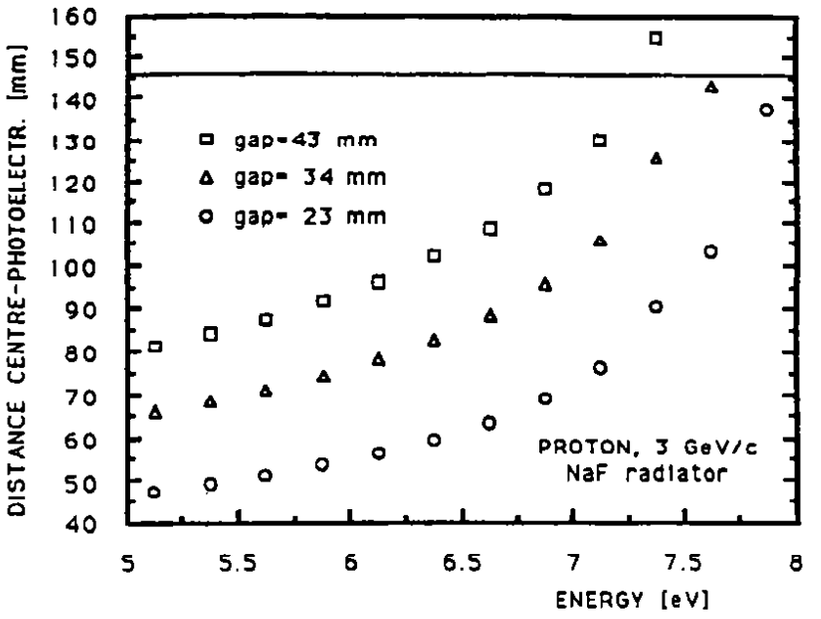

Figure 3: Definition of the fiducial zones for three distances of the radiator-to-pad plane. The boundaries are: 146 mm in distance from the detector size and 8.2 eV in photon energy from the NaF total reflection.

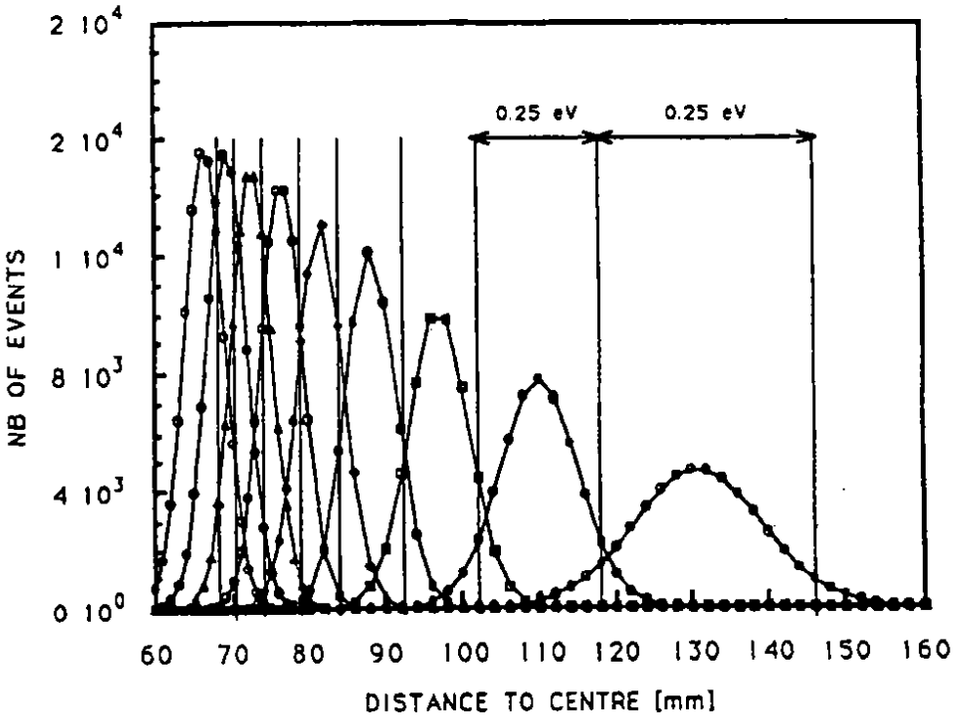

Figure 4: Spread of the photon impacts due to a 10 mm radiator thickness within 0.25 eV energy bins. Calculated for 3 GeV/c protons, distance radiator/pad = 43 mm.

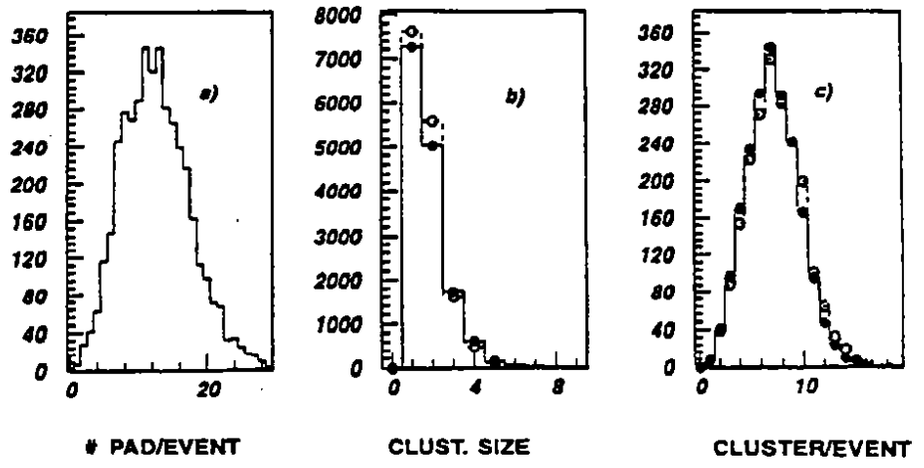

Figure 5: Pad cluster analysis of photoelectrons: (a) Number of pads hit/event; (b) pad cluster size; (c) number of clusters/event. Full and open circles are raw and resolved clusters respectively. The number of entries is 14875 in (b). Experimental distributions from run 50, N = 3.5.

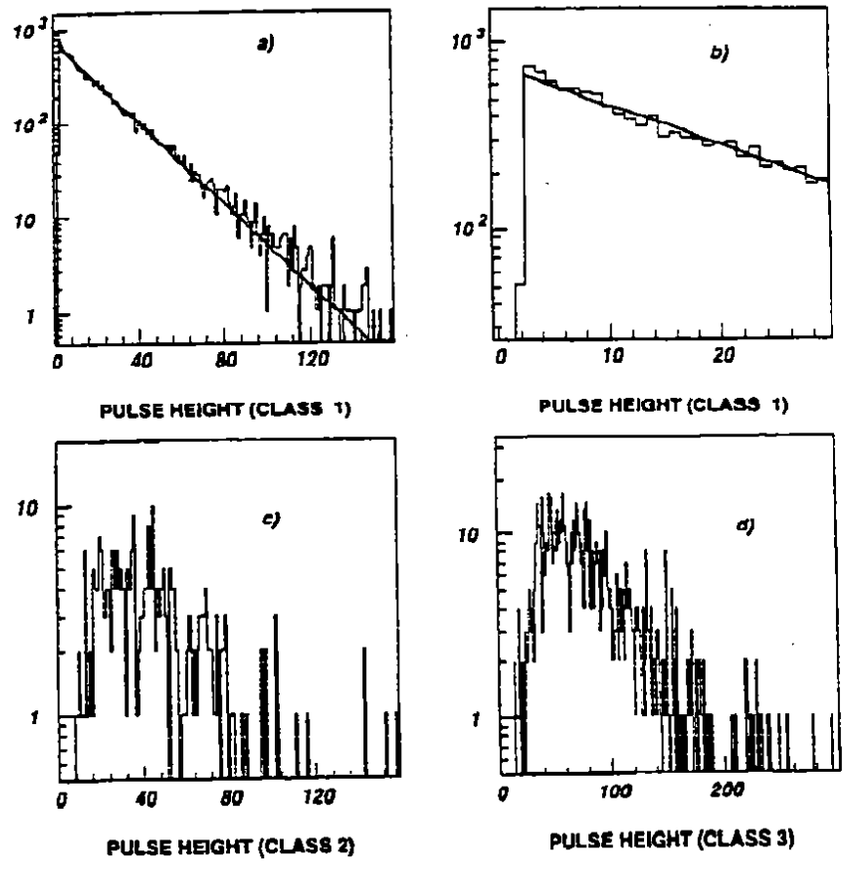

Figure 6: Pulse-height distribution of photoelectrons: (a) Class 1 PH spectrum [13767]; (b) zoom of (a); (c) Class 2 PH spectrum [248]; (d) Class 3 PH spectrum [860]. Number of entries in brackets. Run 50.

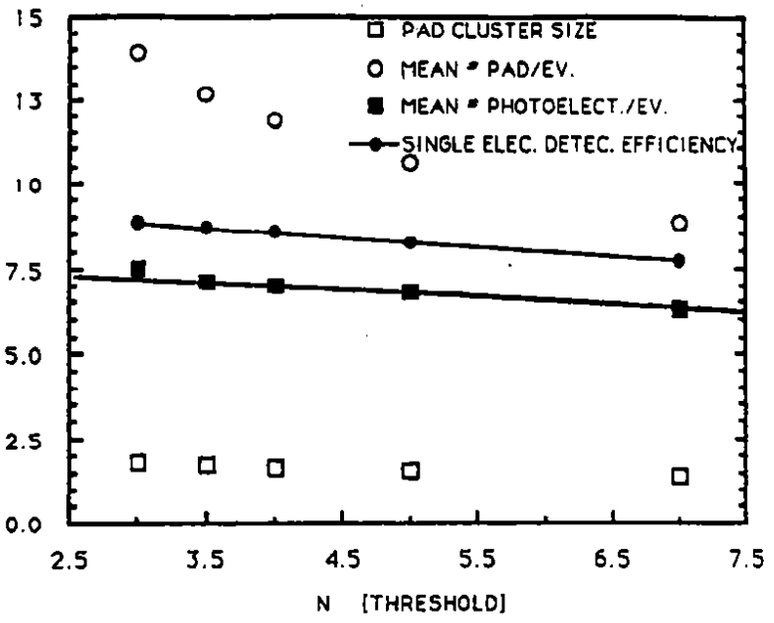

Figure 7: Variation with the pad electronics threshold (N) of the single electron detection efficiency, the number of photoelectrons/event, the cluster size, the number of pads hit/event. The first two curves have the same slopes for N > 3. The vertical scale has to be multiplied by 10 to get the single-electron detection efficiency in per cent.

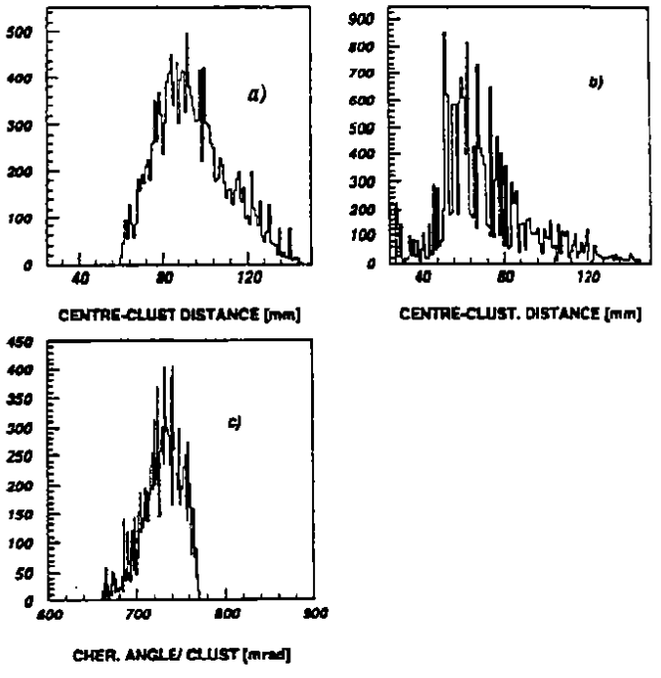

Figure 8: Experimental distributions obtained with photoelectrons: (a) distance to centre, run 50, fiducial zone 60–140 mm; (b) run 18 (methane only), fiducial zone 40–140 mm; (c) Cherenkov angle, as in (a), r.m.s. = 22 mrad. The distance radiator-to-pad plane is 43 mm in (a) and 23 mm in (b).

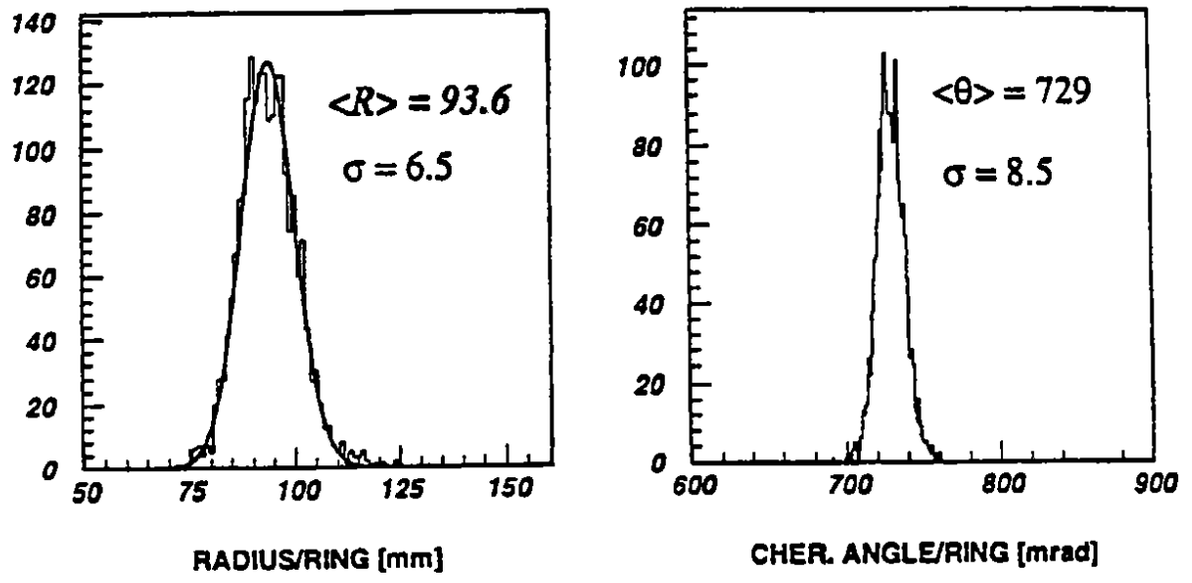

Figure 9: Experimental distributions obtained with rings: (a) radii; (b) Cherenkov angle. Run 50.

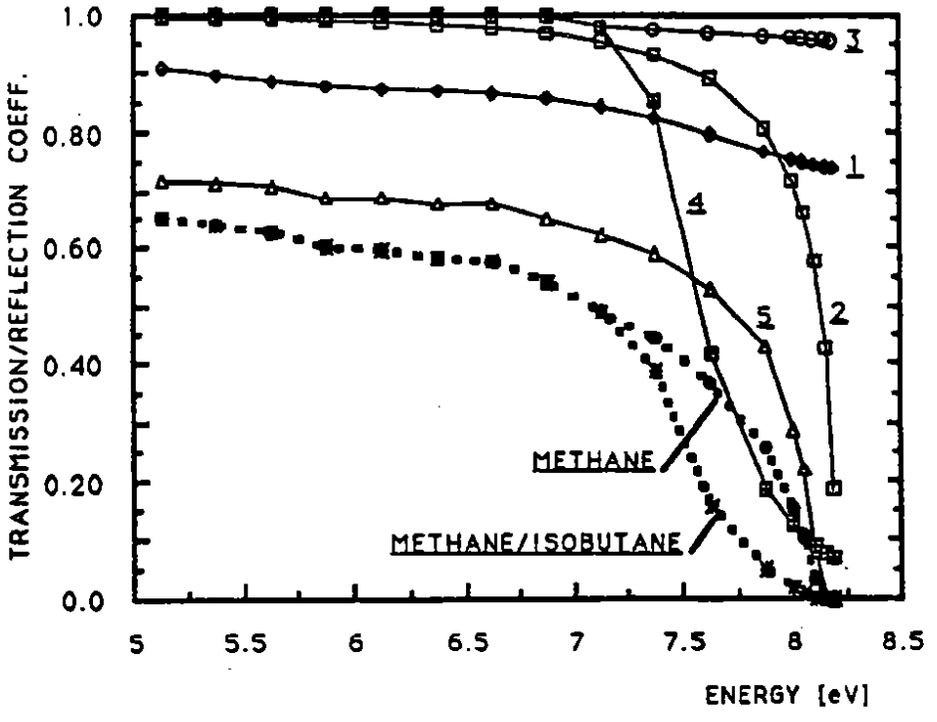

Figure 10: Photon loss curves: 1) measured NaF transmission without reflection loss; 2) calculated reflection loss for p-polarization; 3) methane transmission; 4) methane/isobutane 95/5 transmission; 5) mesh transmission. The calculations are done with 3 GeV/c protons, a 10 mm thick NaF radiator, and a 43 mm thick proximity gap.

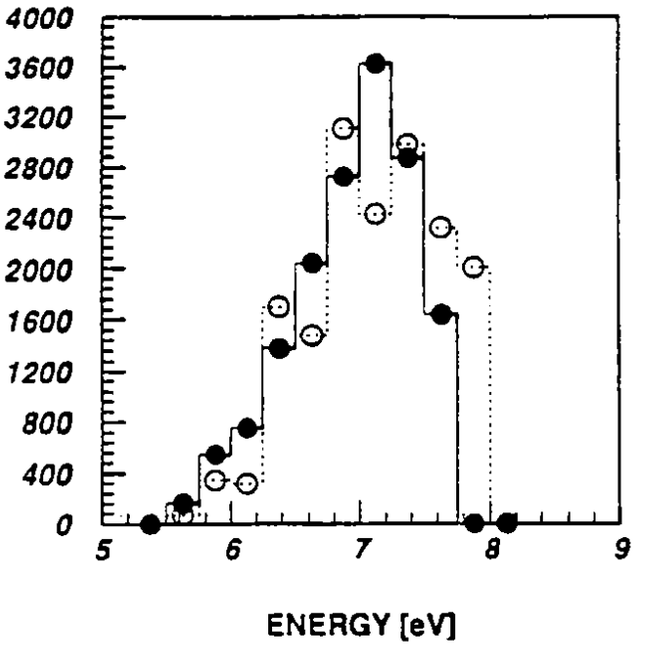

Figure 11: Experimental distributions of the photoelectron frequencies as a function of the photon energy. Full circle: run 50 (methane/isobutane); open circle: run 18 (methane).

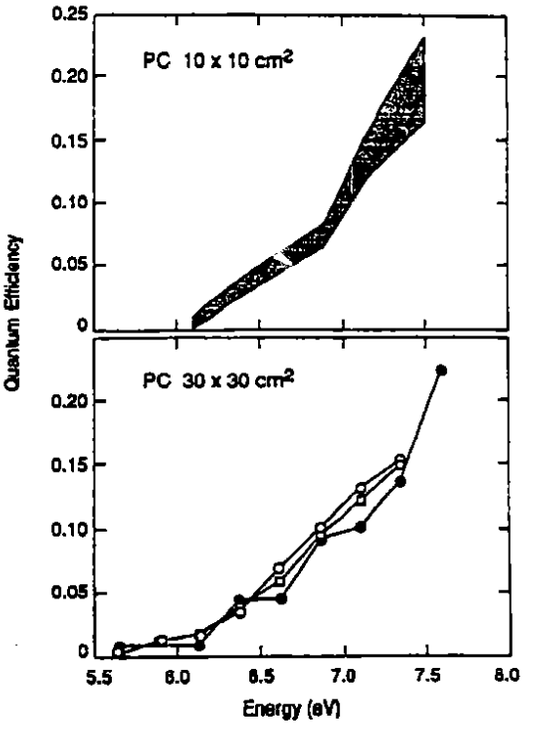

Figure 12: Lower plots: CsI quantum efficiency from runs 18, 50, 52 (full circles, open circles, and squares) respectively. Upper plots: measurements from Ref. [5] re-evaluated with the present analysis.

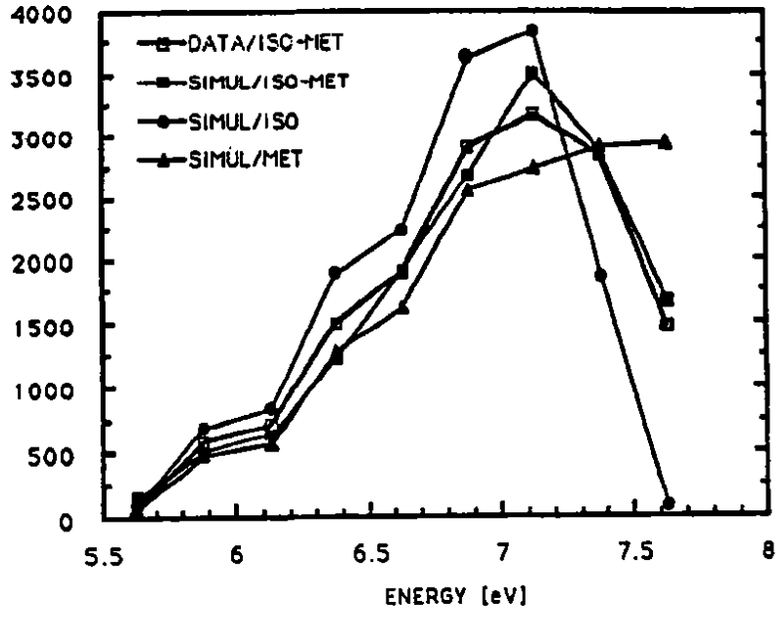

Figure 13: Simulation of the distribution of photoelectron frequencies as a function of the photon energy where the UV transmission curves are taken for three gases: methane, isobutane, and methane/isobutane 95/5. Also plotted: data run 50 obtained with methane/isobutane 95/5.

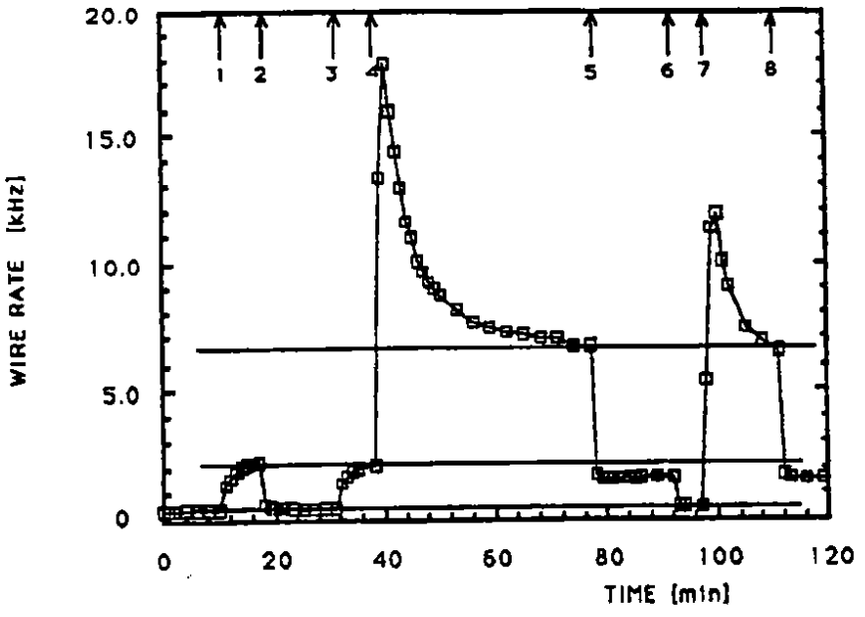

Figure 14: Time variation of the single-electron rate of a pad under UV illumination. The slit widths are: 0.05, 0.12, and 0.28 mm respectively. The arrows indicate when the slit width was either increased or decreased. The plateau levels are indicated by the 3 horizontal lines; the corresponding rates have a parabolic dependence on the slit width.

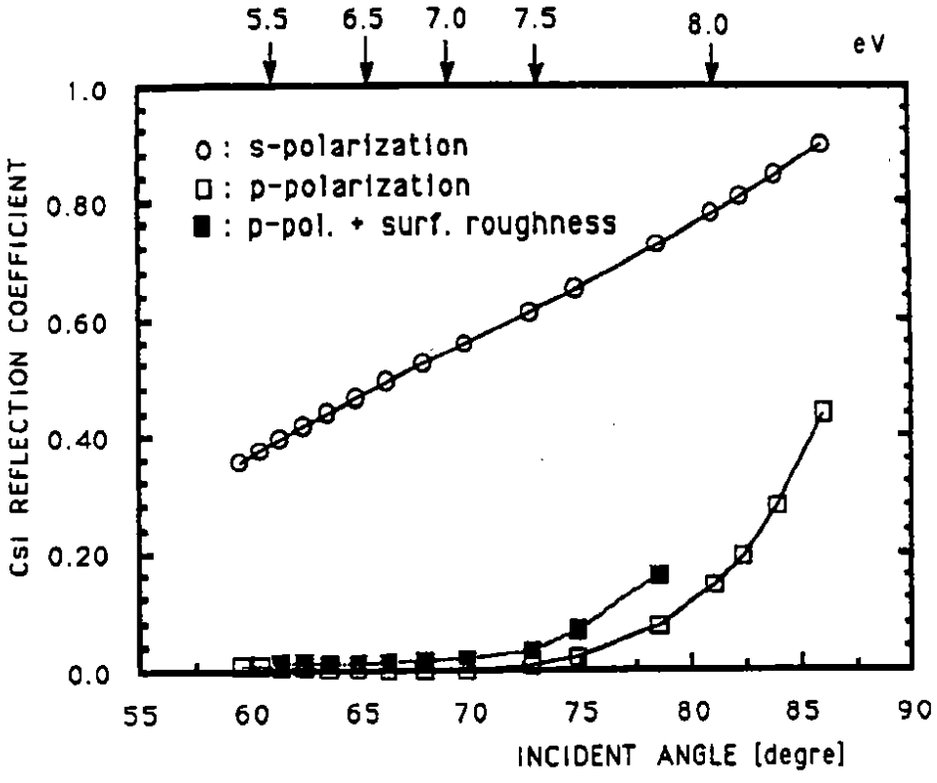

Figure 15: Reflection coefficient at the CsI surface for different polarizations. Calculated for 3 GeV/c protons and a NaF radiator.